46TH TURBOMACHINERY & 33RD PUMP SYMPOSIA
HOUSTON, TEXAS | DECEMBER 11-14, 2017
GEORGE R. BROWN CONVENTION CENTER

Rotordynamic Test Results from a High Flexibility Ratio - High Pressure Fully Instrumented Centrifugal Compressor Test Vehicle

Giuseppe Vannini
CC NPI Rotordynamics Principal Engineer
GE Oil & Gas
Via Felice Matteucci, 2, 50127, Florence, Italy

Emanuele Rizzo
CC NPI Senior Engineer
GE Oil & Gas
Via Felice Matteucci, 2, 50127, Florence, Italy

Antonio Pelagotti
CC NPI Engineering Manager
GE Oil & Gas
Via Felice Matteucci, 2, 50127, Florence, Italy

Carmine Carmicino
Test Lead Engineer
GE Oil & Gas
Via Felice Matteucci, 2, 50127, Florence, Italy

Giuseppe Vannini *is Principal Engineer of the Centrifugal Compressor & Turboexpander New Product Introduction Dept. for GE Oil&Gas, Florence, Italy. Dr. Vannini joined in early 2001. He has been involved in advanced rotordynamics studies on high performance centrifugal compressors developing both analytical and experimental research activities. After leading the first subsea compressor prototype design up to the final FAT he came back to full-time rotordynamic activity and he's active especially in the field of annular seals modeling and testing, advanced gas and oil bearings validation and full scale prototype testing and validation. He holds a PhD in Mechanical Engineering from University of Pisa (Italy) and he's member of API684 Task Force.*

Antonio Pelagotti *is Manager of the Centrifugal Compressor & Turboexpander New Product Introduction Dept. for GE Oil&Gas, Florence, Italy. He's responsible for the development of new technologies for Centrifugal and Axial Compressor.*
Mr. Pelagotti has been with GE Oil & Gas Turbocompressor group since 1999 and has worked as a design engineer, field engineer and application engineer as well as compressor design manager. He has a Bachelor's and Master's Degree in Mechanical Engineering from the University of Florence.

Emanuele Rizzo *is Senior Design Engineer of the Centrifugal Compressor & Turboexpander New Product Introduction Dept. for GE Oil&Gas, Florence, Italy. His current duties are mainly focused on structural design, new material selection and new applications of centrifugal compressors.*
Dr. Rizzo holds an MSc degree (Aerospace Engineering, 2003) and a Ph.D. (Aerospace Engineering, Conceptual Aircraft Design and Structural Design, 2007) from the University of Pisa (Italy). He joined GE Oil&Gas in 2008 as Lead Design Engineer in the centrifugal compressors requisition team, working mainly on high pressure compressors operating in sour environment. He has authored and coauthored several papers on aircraft design and optimization. He is co-inventor in three patents on aeronautics and in three patents on turbomachinery.

Carmine Carmicino *is Project Engineer of the New Product Introduction Turbomachinery Lab for GE Oil&Gas, Florence, Italy. In his current role, he is responsible for the conceptual design of test rigs, instrumentation and acquisition/post-processing systems, analysis, and cost evaluation of assigned projects. Dr. Carmicino holds a MSc degree in Aerospace Engineering and a Ph.D.in aerospace propulsion from the University of Naples "Federico II" (Italy). He worked for the Italian Aerospace Research Center as System Engineer. He joined GE in 2007 as Lead Design Engineer in the centrifugal compressors requisition team, working on LNG, pipeline and high pressure compressors. He has authored more than 40 papers on rocket propulsion, in journals and conference proceedings.*

ABSTRACT

The need for high pressure - high density centrifugal compressors has increased in the recent years due to increased molecular weight found in the new wells. Some compressor OEMs have tested along the years such kind of compressors using state of the art technology (Sorokes et al., Bidaut Y. et al., Tokuyama S. et al., Takahashi, N. et al.). The Authors' Company has recently developed a Centrifugal Compressor Test Vehicle (CCTV) to perform an extensive full speed-full load test campaign focused both to reinforce rotordynamic predictability and to push the current technology boundaries. The CCTV is a dedicated test article configured with a casing designed for 650bar and an interchangeable bundle to easily switch among different test configurations. The CCTV is equipped with special internal instrumentations and devices such as:

- Clearance/vibration probes installed on the honeycomb seal cartridge in order to monitor seal bore tapering in working conditions and measure vibrations on the mid-rotor plane;
- Gas pressure (static and dynamic) and temperature probes in order to measure thermodynamic performance of each stage, to collect secondary flow data for axial thrust investigation and to detect potential aerodynamic induced excitations (rotating stall or surge);
- Thrust bearing equipped with load cells;
- Remote controlled shunt holes line to switch from closed to open state in running conditions.

This test cell is part of a dedicated test loop made by two sections which can be operated both independently (e.g. compressor single stage performance test) and in line (e.g. overall compressor performance test).
The major goal of this activity is to explore the compressor rotordynamic stability for different operating conditions which are representative of all the possible services (e.g. from low density - high speed to low speed – high density) and to eventually set new limits in terms of such parameters. This is in fact the traditional way to setup the rotordynamic experience diagram, see Fulton J.W..
Rotordynamic stability behaviour was assessed through the Operational Modal Analysis approach, (see Baldassarre, Guglielmo et al.), which was made even more effective by the presence of vibration probes on the rotor midplane.
This test program spread over several years and allowed to validate different components and mechanical configurations:

- **Baseline**: direct lube journal bearings, impeller eye laby seals without swirl brakes and tapered honeycomb seal
- **Step#1**: impeller eye laby seal with swirl brakes
- **Step#2**: SFD

The present paper is dealing with the rotordynamic results concerning all the above configurations and the relevant lessons learned.

INTRODUCTION

In the recent years the need for predicting and measuring the stability of a compression system has been more and more important due to the new discoveries of fields with higher content of CO2 so higher molecular weight and finally higher destabilizing forces. Unfortunately many prediction tools are not validated in such condition and many OEMs have built and tested compressors equipped with magnetic exciter to measure the logarithmic decrement, see Sorokes et al., Bidaut Y. et al., Tokuyama S. et al., Takahashi, N. et al.. This OEM has built a CCTV with the aim of measuring the log dec not only in such high density conditions but even at low density in order to have a full picture of rotordynamic behaviour and to be able to ~~select~~ design the best solution for all the possible operating conditions.

TRAIN LAYOUT

As shown by the schematic in Figure 1 the compression train is composed of:

- Gas Turbine (dual shaft). Max power: 10.1MW @ 25°C. MAX speed: 8295rpm.
- Gearbox (parallel axes). Gear Ratio: 1.69.
- Test Vehicle (casing is fixed, bundle can change depending on test scope). MCS: 14000rpm.

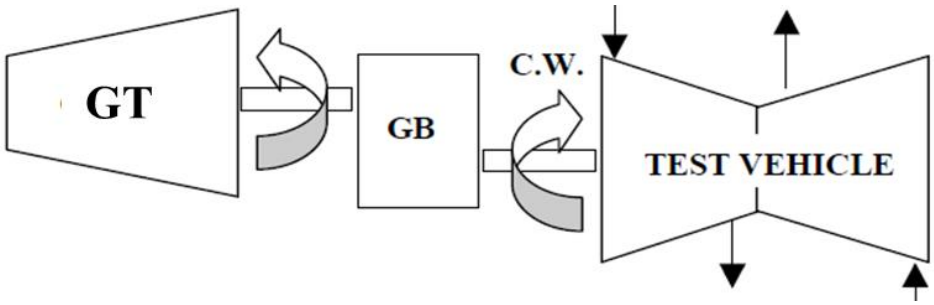

Figure 1 – Train Layout.

TEST LOOP

The test rig is located at the Authors' Company facility in Florence and it is a permanent asset dedicated to Centrifugal Compressor technology, see Figure 2. The test loop around the CCTV is a high pressure industrial plant which is ATEX and PED certified per the state of the art safety regimentation.
At a very general level there are two different sections which serve each compressor section. Through the regulation of a by-pass valve the loop allows to:
- operate the CCTV as an in-line compressor (e.g. two sections in series as in the field)
- test each CCTV section separately (e.g. exploration of a single section compressor performance curve).

Moreover, the presence of a regulating valve for each section allows to change the compressor load (inlet flow) and explore all the required test conditions.
Finally, there is the possibility to open/close the CCTV shunt holes line through a dedicated on/off valve.

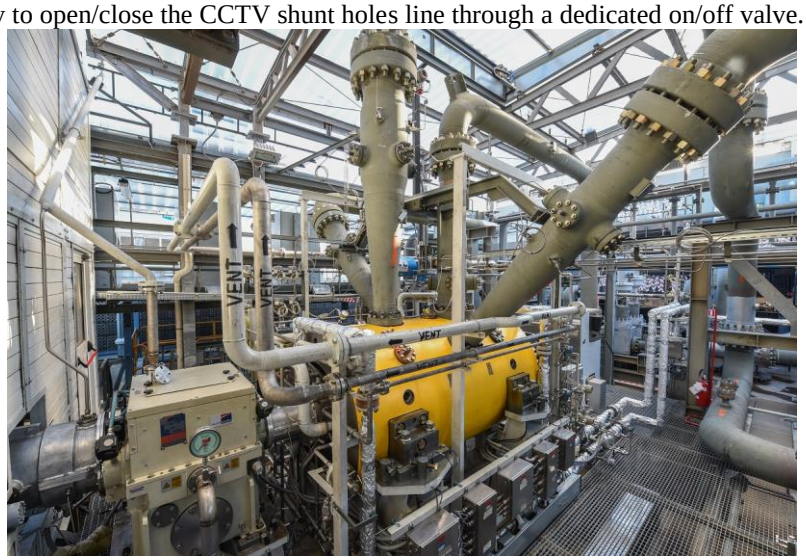

Figure 2- Test Loop.

COMPRESSOR MECHANICAL CONFIGURATION

CCTV is based on a modular compressor casing design. Different bundles can be fit inside depending on the specific test goals (e.g. the operating conditions to be explored or the bearings/seals to be validated). As far as today a back to back rotor was tested (2BCL359/D), see Figure 3.

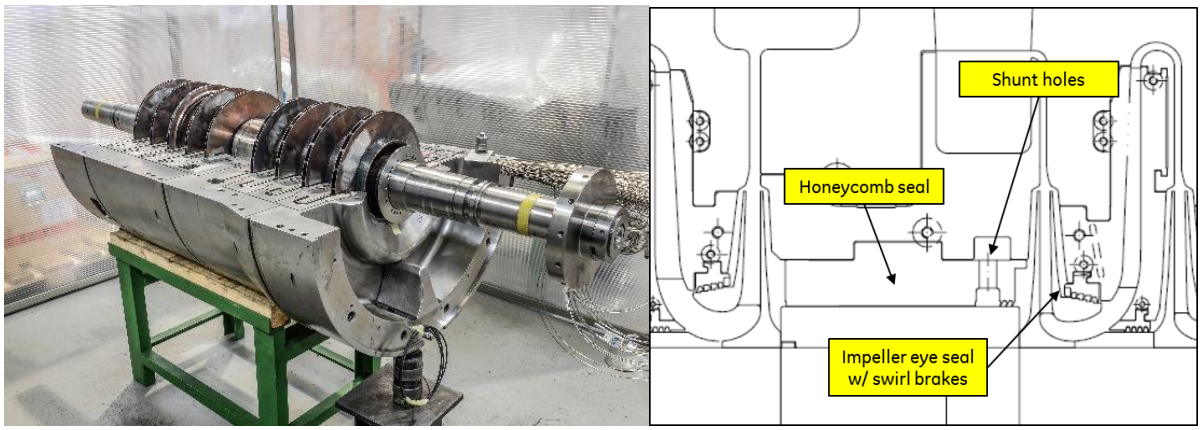

Figure 3 - Left: compressor inner casing and rotor. Right: compressor cross section with details on midspan honeycomb seal.

Main design features are given in Table 1 below. The reason for the large variability of the suction pressure is the need to explore different operating conditions from low density-high speed to high density-low speed.

min Suction pressure (barA)	5
MAX suction pressure (barA)	170
min delivery pressure (barA)	27
MAX delivery pressure (barA)	440
min average density (kg/m3)	10
MAX average density (kg/m3)	300
min Rotational Speed (rpm)	7300
MAX Rotational Speed (rpm)	14000
Journal tip speed (m/s)	35-65

Table 1 – Main design parameters.

The bundle stator is made by an inner casing with diaphragms. Internal seals are mounted on relevant diaphragms and they can be of the following type:

- Labyrinth seal at the impeller eye (with or without swirl brakes) and interstage
- Honeycomb seal at the intermediate balance piston (shunt holes status can be switched on/off on line)
- Abradable seal at the end balance piston

The rotor construction is traditional, made by a solid shaft with shrunk wheels and sleeves.
Journal bearings are one of the major focus of the test so they can be exchanged from one test to another. Up to now the following bearing types have been tested:

- Direct lube tilting pad
- Direct lube tilting pad + SFD

SPECIAL INSTRUMENTATION

In addition to the standard instrumentation such as proximity probes on the journal bearings and on the axial bearing, the compressor internals have been instrumented to a large extent. About 500 probes were installed at the first time, see Figure 4 for a picture of the instrumented bundle. The description of the whole set of instrumentation is out of scope here since the subject is the rotordynamic test. The honeycomb seal located in the middle of the bundle has been instrumented with special probes to measure the rotor-stator clearance,

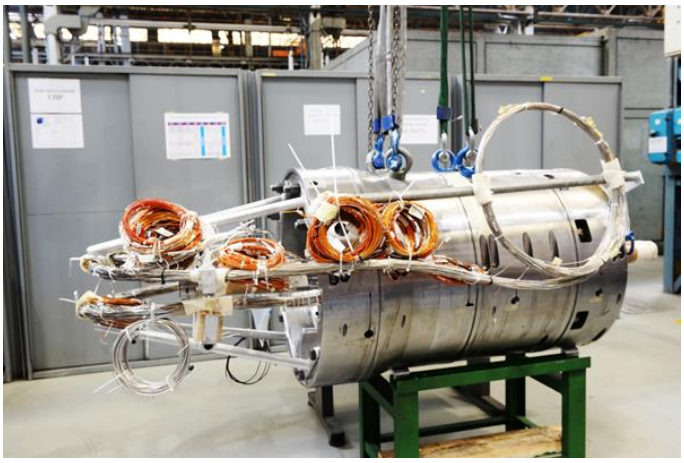

Figure 4 – Compressor bundle with special instrumentation.

The clearance probes are of special interest for rotordynamic purposes. They have a good bandwidth capability so they can be used both for static (clearance) or dynamic (vibration) measurements. Clearances are installed on the honeycomb stator and there are two instrumented planes (the first one at seal inlet and the other one at seal outlet). Four probes per plane are used so there are 8 probes overall. The principle is to measure the stator-rotor gap at two locations 180° out of phase (e.g. A, B) to be able to rule out the rigid displacement (A-B)/2 from the effective seal deformation (A+B)/2. See Figure 5A for a schematic installation layout.
These probes have been selected after a long validation program which led to identify the proper technology and to qualify the best vendor. These probes are not affected by the target material (electrical runout) and they do not have special requirements in terms of surface finishing. Figure 5B shows a clearance measurement during a test point: the inlet clearance was 355micron, the outlet clearance was 313micron so the radial tapering was always positive even at high load (reference is TP#3 shown in the next paragraphs). All the labels are self-explaining except for 1P1 which is compressor suction pressure. Finally Table 2 shows a summary of all the honeycomb seal tapering at operating conditions for each test point (TP) described in the next paragraphs.

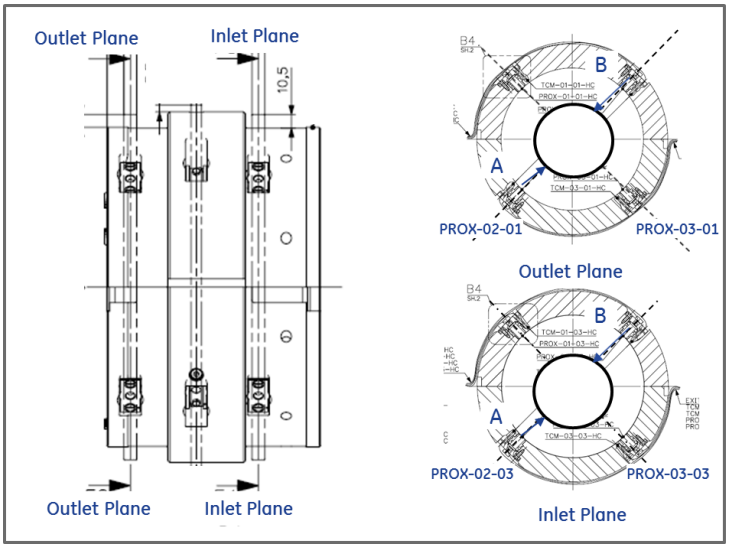

Figure 5-A: Clearance Probe layout.

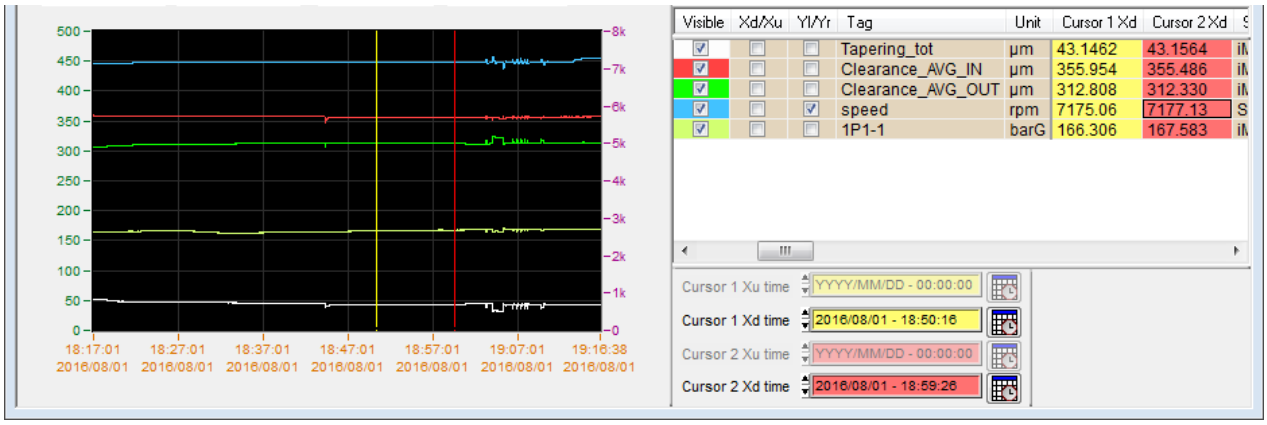

Figure 5–B: Clearance measurement at running conditions.

	Tapering (mm)
TP#1	0.083
TP#2	0.041
TP#3	0.043

Table 2 – Summary of tapering for each of the considered TP.

TEST PROCEDURE

The test is usually performed according to this operative sequence:

- Mechanical Running Test (MRT) at minimum suction pressure and pressure ratio.

Scope of this test is to check the mechanical behaviour up to running speed when the rotor is installed in the test bench for the first time (e.g. after a bundle configuration change or a bearing change). Trim balancing is also performed at this time, if needed.

- Load test according to the target test point (e.g.: to explore a specific point in the rotordynamic experience diagram or to measure a specific performance curve).
- Steady State: after the test point is reached, a steady state condition is then needed before taking any measurement (e.g.: steady conditions within proper specified tolerances are checked for the vital parameters. This means compressor flange pressures, inlet flow, speed etc.).

TEST RESULTS

Foreword

As anticipated, the main object of the test program was the exploration of the rotordynamic experience diagram and the consolidation of the rotordynamic predictability. The target test points were selected in order to cover all the possible market applications in terms of both density and speed: the basic idea was to design a single compressor which was able to cover the most of the conditions of interest, just changing the suction pressure. All the target conditions were finally challenging in terms of rotordynamics so they were very valid points for prediction validation. See figure below where most of the test points explored during the test campaign are plotted into the API617 stability experience diagram as a reference.

In the following paragraphs three different test points are described in full details.

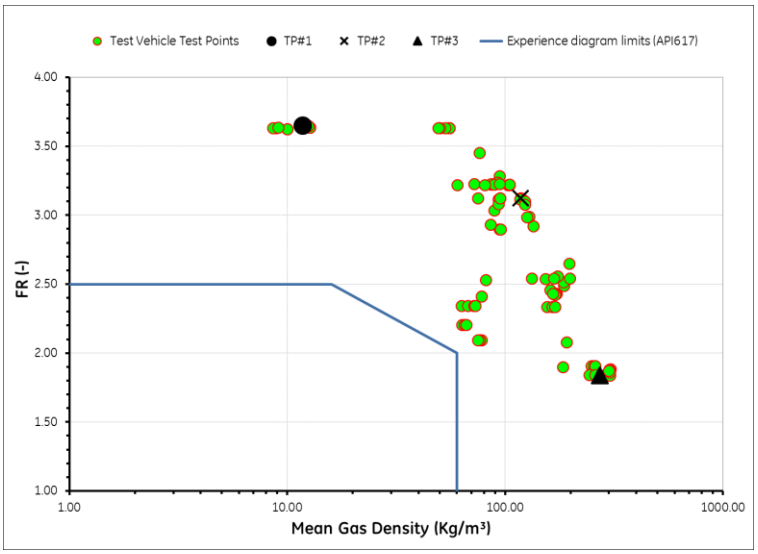

Figure 6 – Stability experience diagram with CCTV test points.

Rotordynamic Design

The compressor rotordynamic analysis is here shortly reported in order to provide a complete scenario for the reader. As shown by the UCS map in Figure 7 the rotor was designed to cross the first two rigid modes and even go beyond the third mode (the first rotor bending mode). The 2nd and 3rd modes are expected to be within the operating range so their responses were checked to stay below the critical damping (Amplification Factor < 2.5 as per API 684 and API 617 requirements).

This rotordynamic design is representative of a "Power Density" compressor which means the thermodynamic selection was optimized to reach the required compression service within the minimum casing size. This means having a final benefit from efficiency, compactness and cost viewpoint. The direct consequence of the size reduction is that the rotational speed increases. Dynamically the rotor crosses the second mode whose response is critically damped (not needing a separation margin) and runs close or above the third mode, depending on bearing clearance.

The maximum achievable flexibility ratio is quite high if compared with the reference value as defined by API617 and API684, see Figure 6 and for this reason the present design is addressed as "high flexibility".

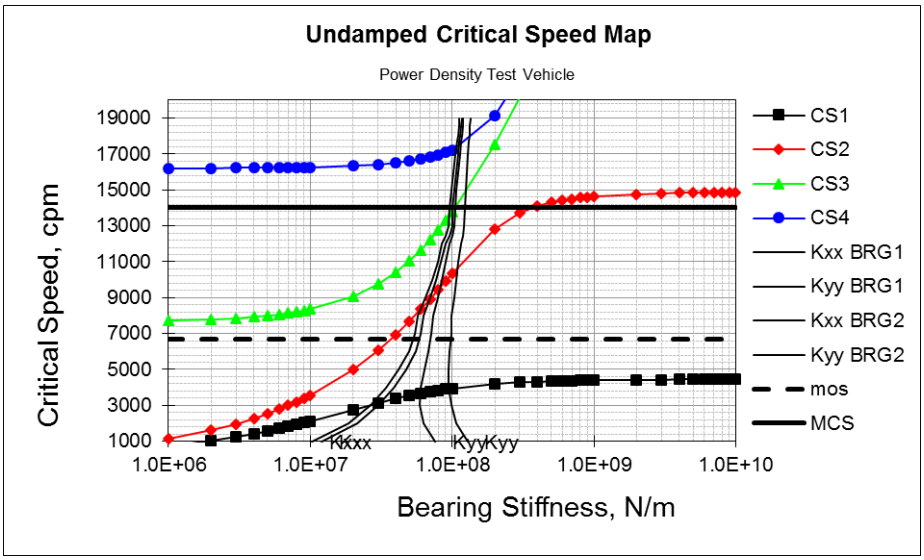

Figure 7 – UCS map.

The journal bearings selected for this task are direct lube tilting pad type, as described in the table below.

Type	Tilting Pad
Lubrication type	Direct
Size (mm)	90
L/D	0.4
N° of pads	5
Load arrangement (on pad/between pad)	On pad
Min diametral clearance (mm) / (/1000)	0.149 / 1.65
Max diametral clearance (mm) / (/1000)	0.187 / 2.073
Preload range	0.2 / 0.4
Offset	50%
Oil type	ISOVG32
Oil inlet temperature (°C)	50

Table 3 - Journal bearing main characteristics.

In order to target the rotordynamic approach described above the bearing clearance was properly selected. This means the bearing stiffness level shall be low enough (compared with the rotor stiffness) that the second and third mode show amplification factors below the critical threshold (AF < 2.5) or, said in other words, the rotor mode shapes shall retain high amplitudes at both bearing locations to get the maximum damping effect.
Finally the rotordynamic stability was checked for all the expected operating points according to API 617 Level 2 requirements and the compressor was found to be stable (log dec > 0.1) thanks to the use of an intermediate honeycomb seal. The option for the shunt holes on the same seal was also taken into account since the test rig is offering the possibility to run with this device alternatively closed or open. As expected the shunt holes enhanced the stability predictions but they were not mandatory for all the operating conditions. More details about the predictions will be shown later in the paragraph dedicated to the comparison with the test results. The following is the list of internal seals which were considered for Stability Level 2 analysis:

- Impeller eye laby seals (TOS laby with no swirl brakes)
- Intermediate honeycomb seal (with or without shunt holes)
- End balance piston abradable seal (TOR laby)

The rotordynamic analysis was fully compliant with API617 requirements and also with the Authors' Company Rotordynamic Design Practice.

Rotordynamic Model Validation
Since the major goal of the test campaign was to check the rotordynamic predictability, the model was validated step by step to minimize the overall error and to rule-out the sources of major uncertainty.
At the beginning the rotor modeling was checked versus ping test results. Rotor construction was fully conventional but this check was anyway useful to quantify the discrepancies relevant to the rotor modeling.

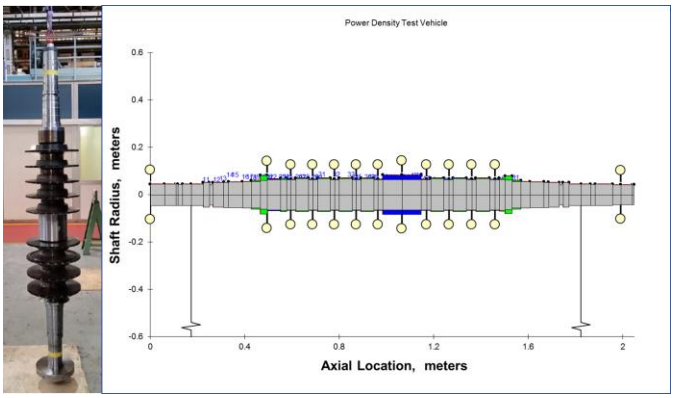

Figure 8 – Rotor Ping Test and rotordynamic model.

Rotor ping test, as usual, was done with the rotor almost fully assembled (only dry gas seals and coupling hub were missing at this stage), and hung in a vertical position (the relevant lifting lug mass was incorporated into the model) in an almost free-free condition. Rotor was instrumented through several accelerometers which were all aligned in the same plane and located in axial key points in order to determine at the best the mode shapes of interest. The focus here was mainly on the first bending mode due to the specific rotordynamic design as shown in Figure 7.

Rotor modelization was done through an available software code (see XLTRC^{2TM}) and according to the Company Authors' Design Practice. Worth of mention here is the stiffening effect of shrunk components (e.g. impellers, sleeves, and balancing drums) which was taken into account to closely match the test data (see Smalley et al.). As shown by Table 4 the model was really accurate for what is concerning the first mode prediction so no error is expected to come from this side. As a side note the first natural frequency is quite different from the one which can be extrapolated from the UCS in Figure 7 (141Hz vs 129Hz). This is because the ping test rotor configuration is not exactly the final one: the coupling hub is missing at that time and this is making the major difference. The first flexible mode shape shows the maximum amplitude at both the shaft ends so it is very sensitive to overhung masses. On the contrary the second bending mode prediction did not show the same level of accuracy but this was not considered as a concern since the machine was supposed to operate far from this mode (at least 15% as per the rotordynamic analysis).

Measured		Predicted		Check	
NF1 (Hz)	NF2 (Hz)	NF1 (Hz)	NF2 (Hz)	Δ NF1 (%)	Δ NF2 (%)
141	282	141	302	0%	+7%

Table 4 – Ping test results vs. predictions.

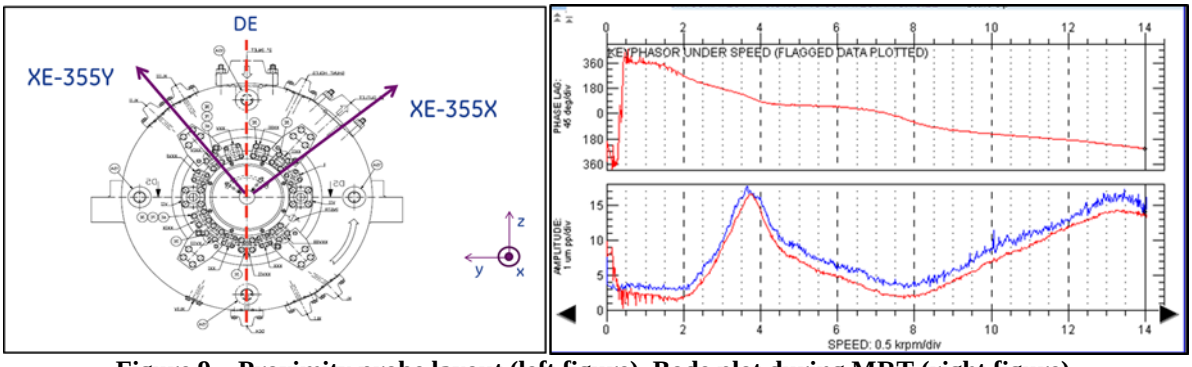

Figure 9 – Proximity probe layout (left figure). Bode plot during MRT (right figure).

As anticipated the first check in the test bench configuration is the MRT. This test confirmed the sound rotordynamic design in terms of both critical speeds position and relevant amplification factors. In fact the first critical speed showed up around 4000rpm and, as expected, the second mode was not visible at all in the Bode plot, while the third mode was close to MCS and very damped as well, see

Figure 9. This figure shows the response measured by the XE-355X proximity probe which was installed close to the drive end bearing.

Table 5 is summarizing the comparison between MRT results and relevant predictions for the first critical speed. The level of agreement is satisfactory being the first critical speed predicted within 5% error (API617 requirement) and the AF predicted close to the experiment value and on the conservative side.

Measured		**Predicted**		**Check**	
CS1 (rpm)	AF (-)	CS1 (rpm)	AF (-)	ΔCS1 (%)	ΔAF (%)
3900	3.5	3812	4.1	-2%	+17%

Table 5 – MRT results vs. predictions.

This check was useful to validate the journal bearing modelization. Bearing coefficients were predicted through an available code developed by University of Virginia (see Branagan and Barrett) which was then optimized based on proprietary test data. This validation was performed leveraging available journal bearing test data (both static and dynamic) coming from an internal test rig, see Delgado, Libraschi et al.

Load Test Results

Rotordynamic stability measurements were performed through Operational Modal Analysis (OMA). The software used for OMA was purchased and validated over several years, see Artemis. This approach was in fact extensively tested and validated both by the Authors' Company, (see Guglielmo et al., Baldassarre, Guglielmo et al.) and also by others, (see Carden). Recently, this approach was compared versus another method based on the use of a magnetic exciter: the two methods showed equivalent results in all the explored pressure (density) range (see Baldassarre, Guglielmo et al.). Namely no specific advantage was coming from the exciter method, at least in the tested operating conditions: low damped modes showed equivalent results and when log dec becomes high (e.g. $\delta > 1$) the mode becomes harder to identify whichever the method. Furthermore, the OMA approach is much less invasive: no need for any additional magnetic device together with relevant shaft spool.

Final step for rotordynamic validation is the effect of compressor load on stability.

In order to predict the rotordynamic stability the following annular seal codes and relevant assumptions were used:

Seal Type	**Code**	**Preswirl**	**Operating Conditions**
Impeller eye laby seals	XLLaby™ [1]	Computed	Test data/Computed
End balance piston abradable seal	XLLaby™	Computed	Test data/Computed
Intermediate honeycomb seal	ISOTSEAL™ [2]	Computed	Test data/Computed

Table 6 – Code and assumptions for internal seals calculations.

It is worth to mention here the seal codes were also subject to an internal validation at component level in the Authors' Company during the last years. This activity led to satisfactory results for what is concerning the laby seal code (see Vannini, Cioncolini et al.) while the honeycomb seal code showed significant discrepancies and required a fine tuning (see Vannini, Mazzali et al.).

For what is concerning the preswirl (which is a vital parameter in seal coefficients evaluation) this was available only through computations since the direct measurement was not available. The computation was done through an internal flow solver which was run cavity by cavity and then tuned based on pressure values where available (first and last cavity of each section were instrumented). This allowed removing arbitrary assumptions. Moreover test data were used as input operating conditions where available (e.g. molecular weight, speed). On the contrary gas pressure and temperature input values (needed for each stage) were computed from the thermodynamic code which was preliminarily calibrated on the compressor flange parameters.

Finally honeycomb seal operating clearances were also available through the dedicated instrumentation, as described in the Special Instrumentation paragraph. It is worth to say the honeycomb seal profile was designed to be always convergent in operation as confirmed by Figure 5 and Table 2. Moreover the honeycomb design (e.g. cell width, void area ratio, depth) and manufacturing process (EDM aluminum) are typically used for all the projects. It is worth to mention that for all the three test points described in details in the following paragraphs the seal configuration was always the same.

1 : see Childs and Scharrer.
2: see Kleynhans.

TP#1

This was the test point with the lowest average density over the entire test campaign and this was achieved with the minimum compressor suction pressure. At the same time the rotational speed was the maximum achievable in the test.
Table 7 shows the comparison between measured rotor modal parameters and best predictions.

Test Point	Rotational Speed	Suction Pressure	Delivery Pressure	Mean Gas Density	Measured*		Predicted	
-	rpm	barg	barg	Kg/m3	NF1 (Hz)	δ (-)	NF1 (Hz)	δ (-)
#1 (shunt holes closed)	14000	5	40	12	75	0.02	66	0.05
#1 (shunt holes open)					74	0.27-0.29	65	0.53

Table 7 – TP#1: stability test results vs. predictions.

*: measured values are provided as a range in order to quantify the experimental variation. The range is defined as min-MAX value from the identification when different methods and signal frequency bandwidths are used.

Predictions were fine-tuned based on seal component level test as shown in details in the next paragraph.
From Table 7 it is possible to appreciate the following major points:
- rotor was marginally stable without shunt holes
- shunt holes had a very positive effect on stability
- measured frequency is higher than predicted, likely due to an error on honeycomb seal stiffness estimation in these specific operating conditions. As a reference for the reader if the direct stiffness were just 3.5 times higher than currently predicted, the measured frequency might be targeted.

About the shunt holes positive effect on stability it is worth to show the change in vibration spectrum for TP#1 when the compressor changed from marginal stable to fully stable, see Figure 10. The waterfall map shows clearly the vibration amplitude at the first natural frequency (around 75Hz) which is suddenly reducing at the time of shunt holes opening.

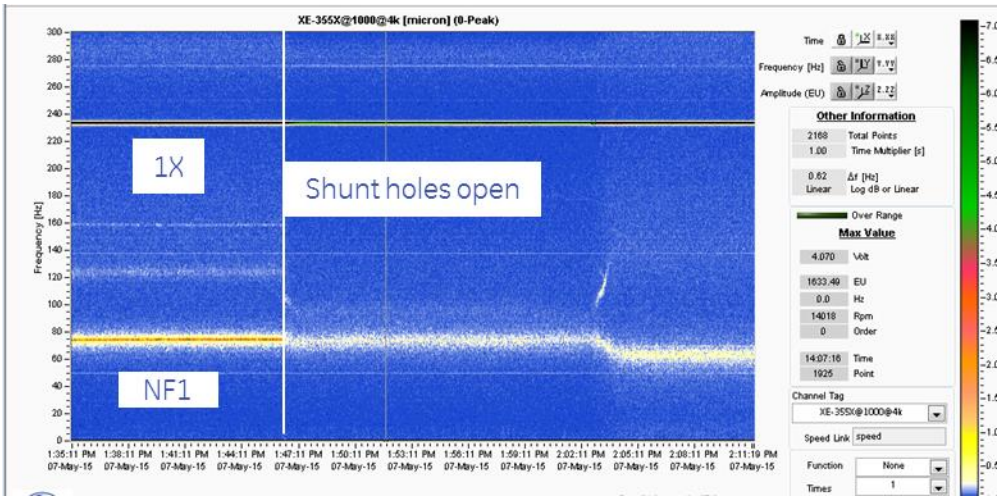

Figure 10 – TP#1 waterfall plot before and after shunt holes opening.

The honeycomb effect on the rotor overall stability is quite low for the present test point (with shunt holes closed). This is related to the low pressure differential across the seal together with the high preswirl which drive the honeycomb to develop even a negative effective damping. The table below shows the split effect predicted for the laby seals and the honeycomb. This is a condition where the stability

may be improved playing mainly on the laby seals and the journal bearings.

Calculation step	δ (-)	NF1 (Hz)	Δ δ (-)	Δ NF1 (Hz)
rotor + brgs.	0.23	64	-	-
rotor + brgs + end balance piston TOR laby + impeller eye labys	0.09	62	-0.15	-1
rotor + brgs + end balance piston TOR laby + impeller eye labys + honeycomb	0.05	66	-0.05	4

Table 8 - Incremental effect of annular seals on rotor stability (TP#1).

Figure 12 shows the level of the predicted coefficients for this TP compared with the other two TPs taken at higher pressure/density level.

TP#2

This test point was based on an average density about 10 times higher than the previous test point. Stability measurements show a stability level much increased together with a significantly lower natural frequency. While the first aspect is already well known in literature from previous experiences (e.g. see Moore at al.) the second aspect is especially interesting. The natural frequency trend is in fact quite against the common sense because the honeycomb seal is very often considered almost as a third support capable to raise the natural frequency, but this is not always the case. Moreover the decreasing trend of natural frequency with gas density is confirmed also by the TP#3 results.

As said, the effect of gas density is to increase stability: as shown by Table 7 and Table 9 there is a factor 10 in δ value identified through OMA between TP#1 and TP#2. Shunt holes effect again is very beneficial for stability driving the δ over 1.

Test Point	Rotational Speed	Suction Pressure	Delivery Pressure	Mean Gas Density	Measured*		Predicted	
-	rpm	barg	barg	Kg/m3	NF1 (Hz)	δ (-)	NF1 (Hz)	δ (-)
#2 (shunt holes closed)	12005	85	165	118	59-60	0.33-0.34	69	0.30
#2 (shunt holes open)					54-57	1.0-1.22	50	3

Table 9 – TP#2: stability test results vs. predictions.

*: measured values are provided as a range in order to quantify the experimental variation. The range is defined as min-MAX value from the identification when different methods and signal frequency bandwidths are used.

Looking at the predicted incremental effect on stability is clear for this test condition the honeycomb effect is now strong and beneficial on δ especially, see table below.

Calculation step	δ (-)	NF1 (Hz)	Δ δ (-)	Δ NF1 (Hz)
rotor + brgs.	0.25	64	-	-
rotor + brgs + end balance piston TOR laby + impeller eye labys	-2.41	67	-2.84	6
rotor + brgs + end balance piston TOR laby + impeller eye labys + honeycomb	0.30	69	2.70	2

Table 10 - Incremental effect of annular seals on rotor stability (TP#2).

It is worth to say the predictions shown in Table 9 are so good in terms of δ (for what is concerning the case with shunt holes closed) because the honeycomb seal coefficients have been fine-tuned leveraging proprietary test data coming from an internal high pressure seal test rig (see Vannini, Cioncolini et al.). It is worth to notice that in the Seal Test Rig tuning case the preswirl level was high. This is the reason why the final predictions are better in the high preswirl case than in the low preswirl case. Following table shows a summary of all the considered preswirl values while Figure 12 shows the predicted coefficients for all the test points considered.

	Shunt holes	
	Closed	Open
TP#1	0.8	0.17
TP#2	1.1	0.26
TP#3	0.9	0.2

Table 11 – Summary table with preswirl values for all the TPs analyzed.

Going more in details the Authors looked back into a test campaign performed on that rig and they identified the most similar seal geometry to the one installed in the Test Vehicle, see Table 12. For this specific seal both the experimental leakage and the rotordynamic coefficients were available to check ISOTSEAL™ predictability.
It is evident from Table 12 that the geometry of the component level tested seal was very similar to the system level tested one except for the length which was about half of the actual. Speed and pressure ratio were also very similar between TP#2 from Test Vehicle and the selected tuning TP from Seal Test Rig campaign. This tuning test point was only one in the whole seal test campaign and it was selected because it showed the maximum level of similarity with respect to the Test Vehicle TP#2 operating conditions. For sure all the considerations presented in the next lines are going to be extended to the whole test campaign in order to make the tuning more general and robust.

	Test Vehicle (TP#2)	Seal Test Rig (tuning TP)	Δ (%)
Diameter (mm)	183	170	-7%
Length (mm)	130	65	-50%
Clearance min. (mm)	0.28	0.33	18%
Cold Tapering (mm)	0.1	0.1	0%
Rotational Speed (rpm)	12300	12000	-2%
Pressure ratio (-)	1.34	1.4	4%
Preswirl (-)	0.95	0.75	-21%

Table 12 - Honeycomb seal comparison.

At first the leakage test data were compared with relevant predictions and the model was tuned within 1% accuracy (see Table 13). The tuning was done changing the statoric friction factor parameters into the predictive code. This parameter in fact may change depending on the honeycomb pattern specific geometry (cell width and depth) and clearance.

	Measured	Original predictions	Tuned predictions
Leakage (kg/sec)	2.01	2.87	1.99
Δ Leakage (%)	0%	42%	-1%

Table 13 - Leakage comparison.

For sake of clarity, the friction factor is used in a seal bulk flow model (e.g. ISOTSEAL™) to simulate the shear forces between gas and metal surface (the honeycomb pattern stator surface in the specific case) so this is governing the leakage prediction at first and ultimately it has an impact on stiffness/damping prediction as well since it is changing the pressure/velocity distribution in the seal.
Many attempts were made in the past by researchers to identify friction factor for honeycomb or hole pattern surfaces (see Childs, Kheireddin, et al.) but Authors decided to leverage proprietary experimental data to get the best estimate.
Second the rotordynamic coefficients were computed based on both original and optimized friction factor and finally compared with experimental data. Figure 11 shows the comparison in terms of both effective stiffness and damping (see Eq. 1 and Eq. 2 for exact

definition). The friction factor tuning had an impact on coefficients and namely it helped to reduce discrepancy on the effective damping (this is easy to understand: friction factor was increased in order to reduce the predicted leakage and this change in turn reflected into a higher predicted damping). On the contrary the friction factor impact on the effective stiffness was not as good as desired since predictions remained higher than measurements.

$$K_{eff} = K_{xy} + C_{xy} \cdot \omega \qquad \text{Eq. (1)}$$

$$C_{eff} = C_{xx} - K_{xy}/\omega \qquad \text{Eq. (2)}$$

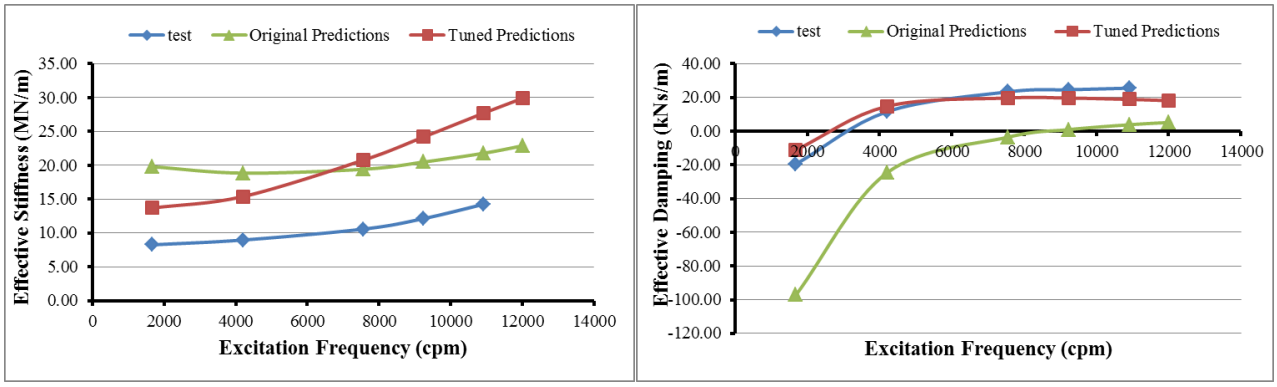

Figure 11 – Seal Test Rig Effective stiffness and damping comparison.

In addition to the friction factor change an additional, experimental tuning coefficient was added in order to improve especially the effective stiffness predictability.

Finally the honeycomb predictions were included in the rotordynamic model and the stability results are reflected by Table 7, Table 9 and Table 14.

Even if the current predictability level is enough for design purposes, at the time of the paper writing the Authors are also working on a more systematic approach: all the available component level test data (coming from the internal seal test rig) will be taken into account and compared on a statistical basis with the relevant predictions coming from the same bulk flow code used here (ISOTSEAL™) or from other predictive tools (e.g. neural networks). The relevant results will be shared as a next step.

TP#3

These test points are characterized by higher density and lower speed trying to address operating conditions typical of a high pressure compressor (usually a high pressure compressor rotordynamic design is based on a low flexibility ratio and for the CCTV case this is achievable just by reducing the rotational speed).

Measured data are more uncertain due to the very high damping level which makes the vibrations on the natural frequency lower in amplitude and harder to detect by the identification algorithm. As anticipated in the previous paragraphs the measured natural frequency for this operating conditions is the lowest at all and this is related to the very high damping level. Stiffness is predicted to be always positive, see also Table 2 for relevant tapering values. From prediction viewpoint the high stability of the compressor is still captured but it was not possible to quantify the exact amount, the relative effect coming from the shunt holes and to compare all this with the relevant predictions. The predictive tool in fact is showing a very high damping when shunt holes are open, and this damping is responsible both for the high log dec and the low natural frequency (e.g. think to a 1DOF mechanical system where the damped natural frequency is given by Eq. 3: the higher damping, the lower the damped natural frequency). Note that the frequency drop from 36Hz to 14Hz is mainly due to the effect of the damping while the stiffness remains at same or even higher level with respect to the case with shunt holes open, see Figure 12.

$$\omega_d = \omega_n \cdot \sqrt{1-\xi^2} \qquad \text{Eq. (3)}$$

All this tuning strategy was finally implemented into the relevant design tools in order to enable a safe design for future centrifugal

compressors running in similar operating conditions.

Test Point	Rotational Speed	Suction Pressure	Delivery Pressure	Mean Gas Density	Measured*		Predicted	
-	rpm	barg	barg	Kg/m3	NF1 (Hz)	δ (-)	NF1 (Hz)	δ (-)
#3 (shunt holes closed)	7200	164	380	272	34-53	>1.5	36	2.3
#3 (shunt holes open)				272	34-47	>1.5	14	8.2

Table 14 – TP#3: stability test results vs. predictions.

*: measured values are provided as a range in order to quantify the experimental variation. The range is defined as min-MAX value from the identification when different methods and signal frequency bandwidths are used. Log dec is not exactly measurable due to the very high damping.

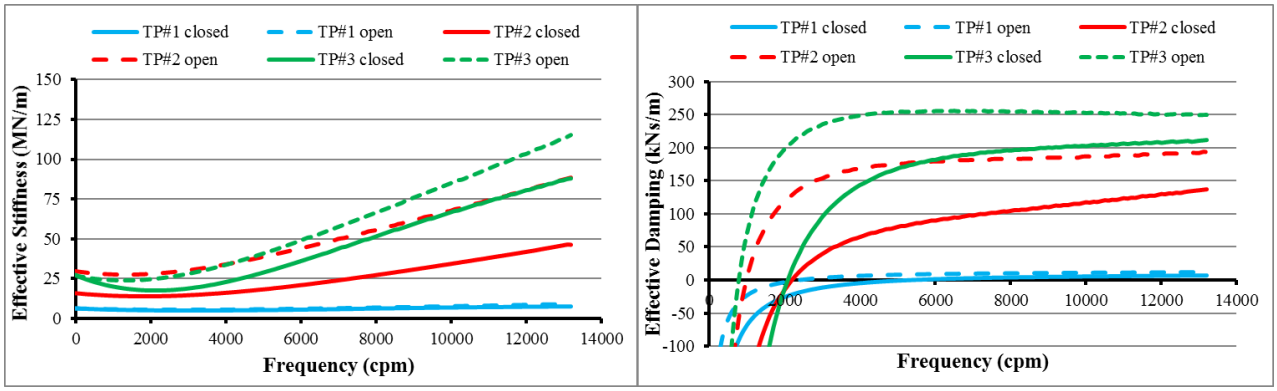

Figure 12 - Predicted effective stiffness and damping for all TPs considered.

Swirl brakes and Integral Squeeze Film Damper

A further step towards the rotordynamic stability improvement was to install impeller eye seals equipped with swirl brakes. This step allowed to quantify the impact of such devices and to tune the preswirl value for future design purposes.

As taught by current literature (see Childs and Baldassarre, Bernocchi et al.) these devices are very beneficial for the rotordynamic stability since they reduce the preswirl value at the seal inlet so they reduce the destabilizing effects from the seal as well. This is a well-known feature in technical literature. What is more interesting is to quantify the impact on the log dec and the proper preswirl level to associate with these devices.

This compressor was equipped with 9 stages so the overall impact of impeller eye laby seals is expected to be huge enough.

The selected test case wasTP#1 since this is the case where the laby seal effect on compressor stability is more evident (honeycomb seal impact on the log dec is very little). Table 15 below shows the final results in terms of log dec.

Swirl brakes	Log dec (-)
NO	0.02
YES	0.22

Table 15 – Swirl brakes OMA results.

A sensitivity analysis with respect to the preswirl value was then performed in order to match OMA results, see figure below.

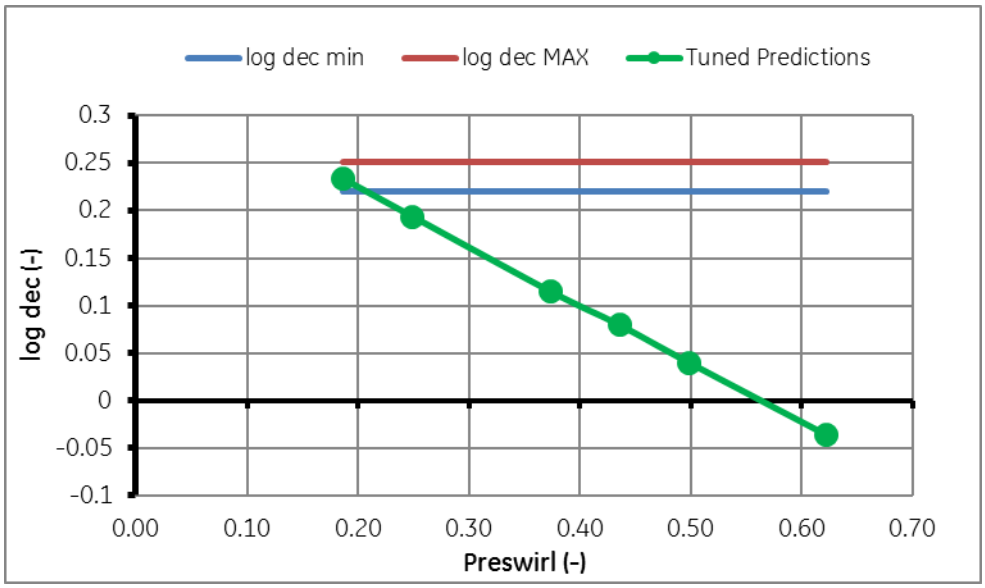

Figure 13 – Preswirl sensitivity analysis.

As a final outcome a 0.2 preswirl value was required in order to match the experimental data. It is interesting to note that a 0.55 preswirl value was applied without swirl brakes. This 0.2 value can be considered as general rule to be used for stability analysis and it is in good agreement with the previous work from Baldassarre, Bernocchi et al. It is worth to notice also that the predicted frequency did not change at all when tuning the preswirl of the impeller eye seals. This is because the laby seal stiffness is very negligible with respect to the rest of the system.

The test rig allowed also to test and verify another critical component in terms of rotordynamic performance: the integral squeeze film damper. This device was used in conjunction with the same 5-pad tilting pad bearing used for all the test activity described so far. The integral squeeze film damper is shown in Figure 14 below and it is a smart invention dating back to '90s (see Zeidan et al.). The Authors' Company started to investigate the benefits associated with this damping device some years ago and carried out a validation activity both at component (see Delgado, Catanzaro et al.) and system level (Gerbet et al.). The final validation was finally possible on the CCTV where the integral squeeze film damper could be tested in site like conditions.

Figure 14 – Integral squeeze film damper installed on the CCTV.

This device is conceptually acting as an additional spring/damper element in series with the oil film spring/damper. The overall beneficial effect on the system log dec is driven by the film/damper stiffness ratio: assuming the bearing design is already optimized and no further

damping is possible to get from there, the damper is introducing a further degree of freedom hence further energy (vibration) to dissipate through damping. Thus, the damper stiffness shall be equal or lower than the bearing stiffness depending on the design target. In this specific case the optimization of the first natural mode log dec was the target so a film/damper stiffness ratio about 4 was selected, see UCS map in Figure 15.

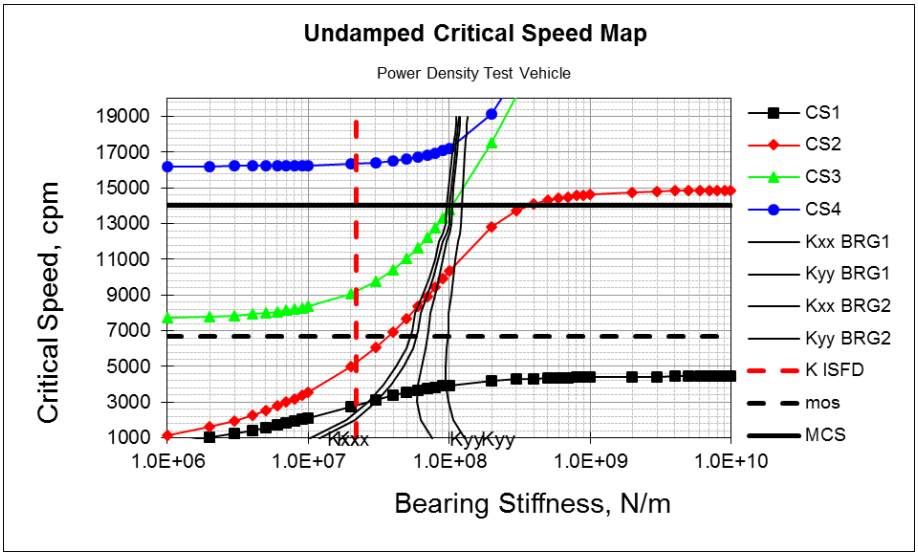

Figure 15 – UCS map with comparison b/w ISFD and bearing film stiffness.

MRT results are summarized in the following figure. Compared with Figure 9 (which is relevant to the rotor response with the traditional tilting pad bearings) the rotor response with the integral squeeze film damper shows a much more damped first critical speed which is in line with the expectations. Response from XE-355X probe was shown for consistency. The rotor is moreover expected to cross second and third mode while running close to fourth mode (still separated). None of these modes is visible from the frequency response due to the huge damping. Vibration level at speed is also in line with API requirements thanks to a trim balancing on the coupling hub. For sure the vibration level at service speed is likely to be higher than with traditional bearings due to the larger flexibility but this shall not be seen necessarily as a concern from an end user viewpoint. This is because the machine is vibrating less at the midspan despite the larger vibration level at the bearings, see Figure 17.

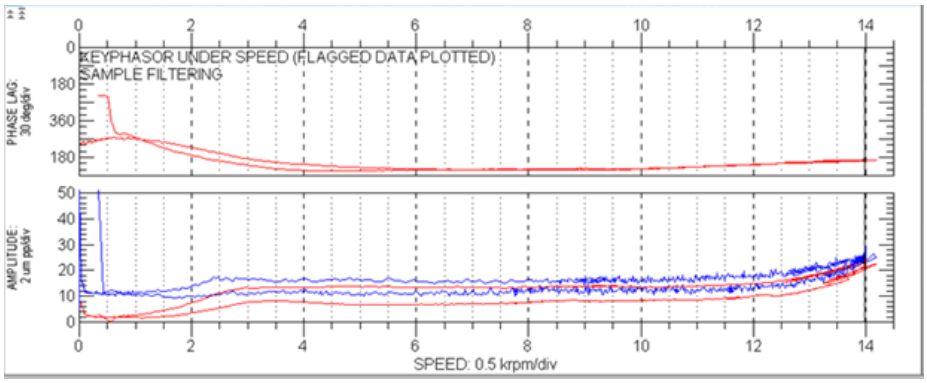

Figure 16 – Bode plot with integral squeeze film damper.

The major outcome of this test is represented by the damping level reached on the first mode which is much higher than the level reached with the use of swirl brakes only, see table below which is relevant to TP#1 operating conditions. As anticipated this was the main target of the present design and it was successfully accomplished, see Table 16. Predictions confirm the log dec is well captured while the

natural frequency is underestimated. The reason is still the lack of prediction of the honeycomb stiffness at these operating conditions.

ISFD	Log dec (-)	Natural Frequency (Hz)
NO	0.22	75
YES	1-1.1	62-64
predictions	0.9	50

Table 16- OMA results with integral squeeze film damper.

The further beneficial implication of having much more damping on the first mode is also having a lower vibration ratio between the rotor midspan plane and the bearing planes: this is an advantage because the internal seals can tolerate tighter clearances. See below the vibration trend during a rotor run-up, XE-355X probe is representative of the vibration at the bearing plane (see Figure 9) while PROX-02-01 is representative of the vibration at the midspan plane (see Figure 5). The bearing/midspan vibration ratio at first critical speed crossing is about 2.5 when using integral squeeze film damper. On the contrary, when using traditional bearings, the vibration ratio is about 3.5.

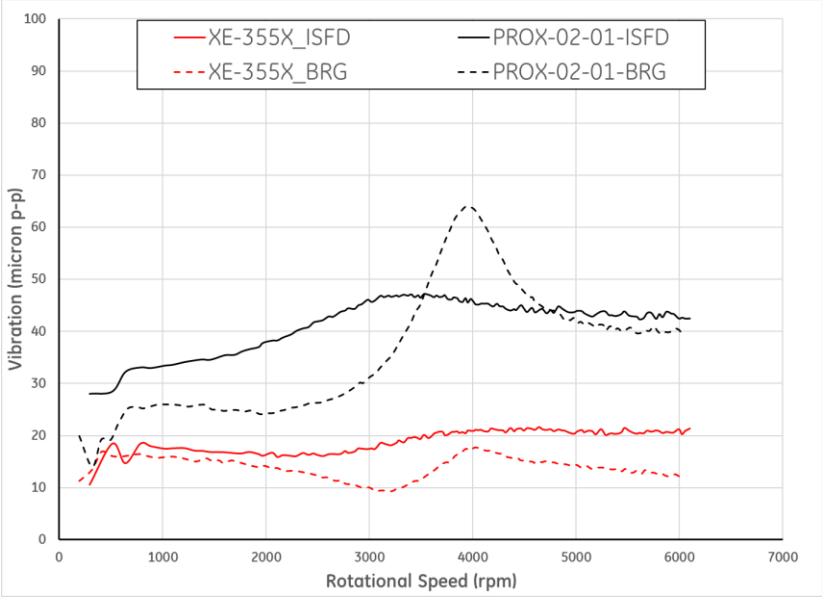

Figure 17 – Bearing vs. midspan vibrations.

This configuration was also tested in the conditions of TP#2 and TP#3 and the integral squeeze film damper effect was only minor: this was because the huge damping already provided by the honeycomb seal.

CONCLUSIONS

CCTV is a live demonstrator of centrifugal compressor technology. The major focus up to now was on rotordynamic predictability for challenging applications where the Power Density concept is needed.
A back to back compressor bundle was tested including the following features:

- Honeycomb seal on intermediate balance piston equipped with shunt holes
- Impeller eye seals with and without swirl brakes
- integral squeeze film damper as an alternative to traditional journal bearings for low density / high speed applications

These features were introduced step by step in order to rule out their single effect.
The activity done so far confirmed the current design capability and allowed to fine tune the predictive tools for such applications. This

tuning will apply to all the future compressor design.
The low density-high speed region test results showed that the destabilizing effects cannot be counteracted using the balance piston damper seal only (even if shunt holes are open): swirl brakes on impeller eyes and integral squeeze film dampers demonstrated to be better options. This last device can be easily adopted with the aim of improving system stability but it needs to be
Rotordynamic predictability in this region is affected by the honeycomb seal (even if this seal is not dominant here) and the gap is more on the effective stiffness side. Shunt holes effect is improving the measured log dec but a further tuning is needed on prediction side in order to limit the effective damping estimation.
Going higher in density showed that a proper honeycomb seal design is able to bring into the system enough damping to guarantee fully stable operations. Worth to mention is the experimental trend of rotor first natural frequency which is dropping down due to the large damping introduced into the system. In addition to this shunt holes are becoming less and less effective. Prediction wise the agreement with the test data is satisfactory when shunt holes are closed since the available tuning database (data from the component level test) is largely based on such condition. If shunt holes are open the predictions tend to overestimate the log dec.
Integral squeeze film damper is a powerful option to stabilize rotors but the higher flexibility introduced in the system needs to be taken into account from design requirement viewpoint: the relevant vibration limits need to be reshaped since this device allows lower vibration levels at rotor midspan when crossing critical speeds.
Finally, as a next step, this test rig will be utilized to explore and validate innovative solutions and operating conditions beyond the current limits of compression technology for Oil&Gas Industry.

NOMENCLATURE

AF	= Amplification Factor	(-)
C	= Damping Coefficient	(N*s/m)
CS1	= First Critical Speed	(rpm)
K	= Stiffness Coefficient	(N/m)
NF1	= First Natural Frequency	(Hz)
NF2	= Second Natural Frequency	(Hz)
P	= Pressure	(bar)
CCTV	= Centrifugal Compressor Test Vehicle	
CF	= Correction Factor	
MRT	= Mechanical Running Test	
OMA	= Operational Modal Analysis	
TOR	= Tooth On Rotor	
TOS	= Tooth On Stator	
TP	= Test Point	
UCS	= Undamped Critical Speed Map	
δ	= Log Dec	(-)
c	= damping ratio	(-)
ω_n	= undamped natural frequency	(rad/sec)
ω_d	= damped natural frequency	(rad/sec)

REFERENCES

API 617, *Axial and Centrifugal Compressors and Expander-Compressors for Petroleum, Chemical and Gas Industry Services*, Eight Edition, September 2014, American Petroleum Institute, Washington, D.C.

API Recommended Practice 684, 2nd edition, 2005, Standard Paragraphs Rotordynamic Tutorial: Lateral Critical Speeds, Unbalance Response, Stability, Train Torsionals, and Rotor Balancing.

Artemis, Software for Modal Analysis, Structural Vibration Soutions, http://www.svibs.com/ .

Baldassarre L., Guglielmo A., Catanzaro M., de Oilveira Zague L., Timbo Silva L., Ishimoto L., Accorsi Miranda M., *Operational Modal Analysis Application For The Measure Of Logarithmic Decrement In Centrifugal Compressor*, Proceedings of the 44th Turbomachinery Symposium, 2015, Houston.

Baldassarre L., Bernocchi A., Fontana M., Guglielmo A., Masi G., *Optimization of swirl brake design and assessment of its stabilizing effect on compressor rotordynamic performance*, Proceedings of 43rd Turbomachinery Symposium, 2014, Houston.

Bidaut Y., Baumann U., Al-Harty S. M. A., R*otordynamic Stability of a 9500psi reinjection centrifugal compressor equipped with a hole pattern seal-measurements versus prediction taking into account the operational boundary conditions*, Proceedings of the 38th Turbomachinery Symposium, 2009, Houston.

Branagan, L. and Barrett, L., *Annex 4 – Tilting pad Dynamic Coefficient Reduction with pivot flexibility*, UVA Report No. UVA/643092/MAE88/376.

Carden E. P., Morosi S., *Operational Modal Analysis of Lateral Rotordynamic Modes of Rotating Machinery*, GT2014-26308, Proceedings of ASME Turbo Expo 2014: Turbine Technical Conference and Exposition, Düsseldorf, Germany, June 16–20, 2014.

Childs D., *Turbomachinery Rotordynamics with Case Studies*, Minter Spring, 2013.

Childs D., Kheireddin B., Phillips S., *Friction Factor Behavior From Flat-Plate Tests Of Smooth And Hole-Pattern Roughened Surfaces With Supply Pressures Up To 84 Bars*, ASME Journal of Engineering for Gas Turbines and Power, April 2011, Vol. 133(9).

Childs, D., Scharrer, J., *An Iwatsubo based solution for labyrinth seals: comparison to experimental results*, ASME Journal of Engineering for Gas Turbines and Power, April 1986, Vol. 108, pp. 325-331.

Delgado A, Catanzaro M , Mitaritonna N, Gerbet M., *Identification of Force Coefficients in a 5-pad Tilting Pad Bearing with an Integral Squeeze Film Damper*, 10th EDF/Pprime Workshop – October 2011.

Delgado A., Libraschi M., Vannini G., *Dynamic Characterization Of Tilting Pad Journal Bearings From Component And System Level Testing*, GT2012-69851, Proceedings of ASME Turbo Expo 2012: Turbine Technical Conference and Exposition Copenhagen, Denmark, June 11–15, 2012.

Fulton J.W., *The decision to full load test a high pressure centrifugal compressor in its module prior to tow-out*, I Mech E., 2nd European congress on "Fluid machinery for the oil, petrochemical and related industries", The Hague, The Netherlands, March 1984.

Gerbet M., Catanzaro M., Alban T., Vannini G., *Rotordynamic Evaluation Of Full Scale Rotor On Tilting Pad Bearings With Integral Squeeze Film Dampers*, GT2012-68745, Proceedings of ASME Turbo Expo 2012: Turbine Technical Conference and Exposition Copenhagen, Denmark, June 11–15, 2012.

Guglielmo, A., Mitaritonna, N., Catanzaro, M. and Libraschi, M., *Full Load Stability Test on LNG Compressor*, GT2014-25353, Proceedings of ASME Turbo Expo 2014: Turbine Technical Conference and Exposition, Düsseldorf, Germany, June 16–20, 2014.

Kleynhans G., Childs D., *The acoustic Influence of Cell Depth on the Rotordynamic Characteristics of Smooth Rotor/Honeycomb Stator Annular Gas Seals*, ASME Journal of Engineering for Gas Turbines and Power, October 1997, 119 (4), pp. 949-957.

Moore J., Walker S., Kudzal M., *Rotordynamic Stability Measurement during Full-Load Full-Pressure Testing of a 6000psi Reinjection Centrifugal Compressor*, Proceedings of 31st Turbomachinery Symposium, Houston, 2002.

Smalley A.J., Pantermuehl P.J., Hollingsworth J.R., Camatti M., *How Interference Fits Stiffen the Flexible Rotors of Centrifugal Compressors*, IFToMM Sixth International Conference on Rotor Dynamics, September 30 – October 3, 2002 - Sydney, Australia.

Sorokes J., Soulas T., Kock J.M., Gilarranz J.L., *Full-Scale Aerodynamic and Rotordynamic Testing for large Centrifugal Compressors*, Proceedings of 38th Turbomachinery Symposium, Houston, 2009.

Takahashi, N., Magara, Y., Narita, M., Miura, H., *Rotordynamic Evaluation of Centrifugal Compressor Using Electromagnetic Exciter*, ASME Journal of Engineering for Gas Turbines and Power, 2012 134(3), pp.032505.1-7.

Tokuyama S., Nakaniwa A., Yoshikazu D., Saburi S., *Development of a High Pressure Ratio and wide operating range 700bar compressor*, Proceedings of 43rd Turbomachinery Symposium, Houston, 2014.

Vannini, G., Cioncolini S., Calicchio V., Tedone F., *Development of an Ultra-High pressure rotordynamic test rig for centrifugal compressors internal seals characterization*, Proceedings of the 40th Turbomachinery Symposium, September 2011, Turbomachinery Laboratory, Texas A&M University, College Station, Texas, pp.46-59.

Vannini G., Mazzali C., Hunderbakke H., *Rotordynamic Computational and Experimental Characterization of a Convergent Honeycomb Seal Tested With Negative Preswirl, High Pressure With Static Eccentricity and Angular Misalignment,* ASME Journal of Engineering for Gas Turbine and Power, May 2017, Vol. 139.

XLTRC2 Rotordynamics Software Suite (2002), Turbomachinery Research Consortium, 2002, Turbomachinery Laboratory, Texas A&M University, Tech. Rep.

Zeidan F., Russel D. I., *Fluid dampened support having variable stiffness and damping*, US 5421655 A.

ACKNOWLEDGEMENTS

The authors recognize GE Oil&Gas Nuovo Pignone for permission to publish the paper and for the opportunity to use the results of CCTV test.

Also warm gratitude is given to all people who made this possible thanks to their daily work in both test stand and control room: Giuseppe Nasca, Stefano Vanghi, Maria Vittoria Borghesi above all.